The Method of Fundamental Solutions for Detection of Cavities in EIT

D. Borman[*], D.B. Ingham[+], B.T. Johansson[#] and D. Lesnic[*]

[*]Department of Applied Mathematics, University of Leeds, Leeds LS2 9JT, UK

[+]Centre for Computational Fluid Dynamics, University of Leeds, Leeds LS2 9JT, UK

[#]School of Mathematics, University of Birmingham, Birmingham B152TT

Emails: d.j.borman@leeds.ac.uk, d.b.ingham@leeds.ac.uk, b.t.johansson@bham.ac.uk, amt5ld@maths.leeds.ac.uk

Abstract: *In this paper, the method of fundamental solutions (MFS) is developed to solve numerically an inverse problem which consists of finding an unknown cavity within a region of interest based on given boundary Cauchy data. A range of examples are used to demonstrate that the technique is very effective at locating cavities in two-dimensional geometries for exact input data. The technique is then developed to include a regularisation parameter that enables cavities to be located accurately and stably even for noisy input data.*

Keywords. *Electrical impedance tomography, inverse problem, method of fundamental solutions.*

1 Introduction

Electrical Impedance Tomography (EIT) is a technique in which an image of the permittivity, or conductivity, of the interior of an object is inferred from surface measurements of electrical phenomena. Practically, this can be achieved by attaching conducting electrodes to the boundary of a person or object and applying small alternating currents to some or all of the electrodes. The resulting voltages are measured, and the process repeated for numerous different configurations of applied current. The electrical potential produced across the object containing the cavity depends on the particular location and the electrical properties of the cavity and, as such, it should be possible to use boundary measurements of the voltage to detect and locate such cavities [Hanke and Bruhl 2003, Holder 2005]. This allows an approximate image of the spatial distribution of the electrical conductivity within the object to be constructed [Borcea 2002].

As a non-invasive technique, EIT can be of particular benefit when it is used for medical imaging. The process uses no ionising radiation, and therefore, it is possible to use the procedure for continuous monitoring. The problem of recovering the conductivity information is a nonlinear and ill-posed inverse problem. As such, one of the current drawbacks to the technique is a low spatial resolution [Boone 2006].

We consider the inverse problem of determining an unknown conductor D compactly contained in a

bounded domain $\Omega \subset \mathbb{R}^d$, d = 2,3, i.e. $\overline{D} \subset \Omega$, entering the Laplace equation

$$\nabla^2 u = 0 \quad \text{in } \Omega \setminus \overline{D}, \text{ with } u|_{\partial D} = 0, \tag{1}$$

from the knowledge of a single Cauchy pair of nontrivial data (u , $\partial_n u$) on the boundary $\partial\Omega$ of Ω, where n is the outward unit normal to $\partial\Omega$ and u is the electrical potential. This type of mathematical model appears in many applications of electric field sensing [Smith 1996, Smith et al. 1998]. In EIT, the homogeneous condition $u|_{\partial D} = 0$ means that the inclusion D is a perfect conductor, i.e. of infinite conductivity.

It has been shown in earlier work [Borman et al. 2007] that the MFS procedure is a technique that accurately approximates the direct problem solution in both two- and three-dimensions and it will be developed in this paper for solving numerically the inverse problem of unknown cavity D identification entering in (1).

2 Mathematical Formulation

Let us state the inverse problem more mathematically. Let Ω and D be bounded domains with smooth boundaries such that $\overline{D} \subset \Omega$, and $\Omega \setminus D$ is connected. Let $f \in H^{1/2}(\partial\Omega)$ be given applied voltage potential, not identically zero. Then the f generates the electric field $\underline{E} = -\nabla u$, where the electric potential u satisfies the following Dirichlet problem:

$$\nabla^2 u = 0 \qquad \text{in } \Omega \setminus \overline{D}, \tag{2}$$

$$u = 0 \qquad \text{on } \partial D, \tag{3}$$

$$u = f \qquad \text{on } \partial\Omega. \tag{4}$$

Note that if the inclusion D is an insulator, i.e. of zero conductivity, then condition (3) should be replaced by $\partial_n u = 0$ on ∂D.

When D is known, it is well-known that the Dirichlet problem for the Laplace equation, as given by equations (2) - (4), has a unique solution $u \in H^1(\Omega)$. Then we can define a nonlinear operator F_f, which maps from the set of admissible subdomains D to the data space of Neumann values in $H^{-1/2}(\partial\Omega)$ as follows:

$$F_f(D) := \partial_n u|_{\partial\Omega} = g \in H^{-1/2}(\partial\Omega). \tag{5}$$

Then the inverse problem under consideration consists of extracting some of the useful information about the domain D from the data $F_f(D)$. As opposed to the direct problem, the inverse problem is nonlinear and ill-posed. The issue of uniqueness, i.e. the identifiability of an unknown perfectly conducting curve ∂D from the Cauchy data ($f \not\equiv 0, g$) on $\partial\Omega$, can be found in [Kress 2004]. The uniqueness can also be established for the identifiability of an unknown perfectly insulated curve ∂D from the Cauchy data ($f \not\equiv$ *constant*, g) on $\partial\Omega$ with $\int_{\partial\Omega} g\,ds = 0$, [Haddar and Kress 2005]. Stability estimates were obtained in [Alessandrini and Rondi 2001].

Since the response operator F_f is a highly nonlinear function of the domain D, extracting useful information from the measurements is a difficult computational problem. If one is interested only in the location of D, then one can employ efficiently the plane or sphere search method for tracking the position of a two- or three-dimensional cavity D, respectively, as described in [Kim et al. 2002]. On the other hand, if the location, shape and size of the obstacle D are all of interest then one can use iterative schemes which require the solution of many forward problems for each change of geometry and position of D, see e.g. [Duraiswami et al. 1997]. These authors used the Boundary Element Method (BEM) as a direct solver, and it is the purpose of this paper to develop instead, for the first time, the MFS, due to its advantages over the BEM, that stem mostly from the fact that the pointisation of the boundary is needed only, which completely avoids any integral evaluation, and makes no significant difference in coding between the two- and the three-dimensional cases [Burgess and Mahajerin 1984, Fairweather and Karageorghis 1998].

3 The Method of Fundamental Solutions (MFS)

The MFS is a member of a class of boundary-type techniques that involve computations being undertaken with respect to points on the boundary of the region of interest. As such, they do not involve interior points of the region of interest, which is useful in many real world engineering applications. Like the BEM, the MFS is an effective technique for solving linear elliptic partial differential equations with constant coefficients for which a fundamental solution is available in explicit form, such as the Laplace, biharmonic and Helmholtz equations. It is a form of indirect boundary integral equation method and a technique that uses boundary collocation or boundary fitting [Johnston and Fairweather 1984]. Based on density results for linear elliptic partial differential equations [Bogomolny 1985], in the MFS we seek an approximation to the solution of the Laplace equation (1) as a linear combination of fundamental solutions, namely,

$$u(\underline{x}) \approx U_N(\underline{x}) = \sum_{j=1}^{N} C_j G_d(\underline{x}, \underline{y}_j), \qquad \underline{x} \in \overline{\Omega} \setminus D, \tag{6}$$

where G_d is a fundamental solution of the Laplace equation in $\mathbb{R}^d$ given by

$$G_d(\underline{x},\underline{\xi}) = \begin{cases} -\dfrac{1}{2\pi}\ln|\underline{x}-\underline{\xi}|, & \text{if } d=2, \\ \dfrac{1}{4\pi|\underline{x}-\underline{\xi}|}, & \text{if } d=3, \end{cases} \tag{7}$$

and the singularities $(\underline{y}_j)_{j=\overline{1,N}}$ are located in $D\cup(\mathbb{R}^d\setminus\overline{\Omega})$. In the first instance, we adopt the simpler version of the MFS, usually called the charge simulation method [Golberg and Chen 1997], in which part of the singularities are known at fixed positions on an artificial boundary located outside $\overline{\Omega}$. The price to pay for not allowing the singularities to move in an adaptive and optimal way is that the location of the fixed artificial boundary has to be dealt with heuristically [Balakrishnan and Ramachandran 2000], although [Bogomolny 1985] suggested that theoretically the locations of singularities can be restricted to any surface embracing $\overline{\Omega}$. The remaining singularities are located in *D* and they are moving with the unknown object *D* throughout the iterative process described below.

In the direct problem given by equations (2)-(4), in which *D* is known, the unknown coefficients $(\underline{C}_j)_{j=\overline{1,N}}$ in equation (6) are determined by imposing the boundary conditions (3) and (4). However, in the inverse problem (IP), given by equations (2)–(5), *D* is unknown. Let us consider a star shaped cavity *D* (with respect to the origin) whose boundary admits the polar (if *d*=2), or the spherical (if *d*=3) parametrizations

$$r = r(\theta), \qquad 0 < \theta \leqslant 2\pi, \tag{8}$$

or,

$$r=r(\psi,\theta), \qquad 0 < \psi \leqslant \pi,\ 0 < \theta \leqslant 2\pi, \tag{9}$$

respectively. Without reducing the generality of the problem we may assume that Ω is the unit circle (if *d*=2), or the unit sphere (if *d*=3).

For simplicity, let us consider the two-dimensional case. Based on expression (8), the boundary of *D* is pointified by

$$r_i = r(\theta_i), \qquad i=\overline{1,M}, \tag{10}$$

where $\theta_i = 2\pi i/M$, $i=\overline{1,M}$.

Then the coefficients $(\underline{C}_j)_{j=\overline{1,N}}$ and the radii $(\underline{r}_i)_{i=\overline{1,M}}$ can be determined by imposing the

boundary conditions (3)-(5) in a nonlinear least-squares sense which recasts into minimising the function

$$S(\underline{C}, \underline{r}) := \| U_N - f \|^2_{H^{1/2}(\partial\Omega)} + \| \partial_n U_N - g \|^2_{H^{-1/2}(\partial\Omega)} + \| U_N \|^2_{L^2(\partial D)}. \quad (11)$$

A few remarks about this function are worth mentioning at this stage:

(i) In the discretised version of (11), for technical computational reasons, we consider all the norms in L^2.

(ii) The constraints $0 < r_i < 1$, $i = \overline{1, M}$, are imposed during the iterative procedure by adjustment at each iteration ($\partial\Omega$ is the unit circle).

(iii) The current flux Neumann data (5) comes from practical measurements which are inherently contaminated with noisy errors and therefore, we replace g in (11) by g^{ε}, where

$$\| g^{\varepsilon} - g \|_{L^2(\partial\Omega)} \leqslant \varepsilon. \quad (12)$$

Based on the above remarks, it is natural to propose minimising the modified discretised objective cost function

$$S(\underline{C},\underline{r}) := \sum_{i=1}^{M} [U_N(\underline{x}_i) - f(\underline{x}_i)]^2 + \sum_{i=1}^{M} [\partial_n U_N(\underline{x}_i) - g^{\epsilon}(\underline{x}_i)]^2 + \sum_{i=M+1}^{2M} [U_N(\underline{x}_i)]^2, \quad (13)$$

where

$$\underline{x}_i = (\cos(\theta_i), \sin(\theta_i)), \quad i = \overline{1, M}, \quad (14)$$

are boundary collocation points uniformly distributed on $\partial\Omega = \partial B_2(0,1)$, and

$$\underline{x}_{i+M} = (r_i \cos(\theta_i), r_i \sin(\theta_i)), \quad i = \overline{1, M}, \quad (15)$$

are boundary collocation points on ∂D. Essentially, we have M collocation points taken on the outer boundary $\partial\Omega$ and M on the inner boundary ∂D of the cavity. It remains to specify the position of the singularities $(y_j)_{j=\overline{1,N}}$ in $D \cup (\mathbb{R}^2 \setminus \overline{\Omega})$. These are taken as

$$\underline{y}_j = (R_{ext}\cos(\tilde{\theta}_j), R_{ext}\sin(\tilde{\theta}_j)), \quad j = \overline{1, N_1}, \quad (16)$$

$$\underline{y}_{j+N_1} = (\frac{r_j}{s}\cos(\tilde{\theta}_j), \frac{r_j}{s}\sin(\tilde{\theta}_j)), \quad j = \overline{1, M}, \quad (17)$$

where $s>1$, $R_{ext}>1$, $\tilde{\theta}_j = 2\pi j/N_1$ and $N = N_1 + M$.

Typically, the values of R_{ext} and s are taken as 2, meaning N_1 singularities are located at a radii twice that of the outer boundary and M singularities are located at a radii half that of the internal boundary.

In equation (13), U_N is given by (6) from which the normal derivative can be calculated as

$$\partial_n U_N(x) = \sum_{j=1}^{N} C_j \, \partial_{n(x)} G_d(\underline{x}, \underline{y}_j), \qquad \underline{x} \in \partial\Omega, \tag{18}$$

where from (7)

$$\partial_{n(x)} G_d(x, \xi) = \begin{cases} -\dfrac{(\underline{x}-\underline{\xi})\cdot\underline{n}}{2\pi|\underline{x}-\underline{\xi}|^2}, & if\ d=2, \\ -\dfrac{(\underline{x}-\underline{\xi})\cdot\underline{n}}{4\pi|\underline{x}-\underline{\xi}|^3}, & if\ d=3. \end{cases} \tag{19}$$

The minimisation of the objective function (13) is performed computationally using the NAG routine E04FCF, which is a comprehensive algorithm for finding an unconstrained minimum of a sum of squares of m nonlinear functions in n variables, where no derivatives are required to be provided by the user, being calculated internally by the routine using forward finite differences.

The approach assumes that the cavity is star shaped and defined by M radii and the centre located at the origin, meaning that this will provide M unknowns to be found during the minimisation. In addition, the MFS procedure requires the vector of coefficients $\underline{C}$ to be found during the minimisation, i.e. the number of additional unknowns will be $N=M+N_1$. The total number of unknowns to be found therefore, becomes $M+N = 2M+N_1$. The least squares minimisation (13) provides $3M$ equations. Since the number of equations must be greater or equal than the number unknowns then this requires $3M \geq 2M + N_1$, or $M \geq N_1$.

An important point to finally note is that the gradient of the function (13) can be calculated analytically. In section 4 we will take $N_1=M$ and this means we have $3M$ unknowns and $3M$ equations, hence $\theta_j=\tilde{\theta}_j$ for $j=\overline{1,M}$. We can re-write (13) explicitly as

$$S(\underline{C},\underline{r}) := \sum_{i=1}^{M} \left[\frac{1}{2} \sum_{j=1}^{M} C_j \ln[1+R_{ext}{}^2 - 2R_{ext}\cos(\theta_i-\theta_j)] \right. \quad +$$

$$\left. \frac{1}{2} \sum_{j=M+1}^{2M} C_j \ln\left[1+\left(\frac{r_{j-M}}{s}\right)^2 - \frac{2r_{j-M}}{s}\cos(\theta_i-\theta_{j-M})\right] - f(\cos(\theta_i),\sin(\theta_i)) \right]^2$$

$$+\sum_{i=M+1}^{2M}\left[\sum_{j=1}^{M} C_j \frac{1-R_{ext}\cos(\theta_{i-M}-\theta_j)}{1+{R_{ext}}^2-2R_{ext}\cos(\theta_{i-M}-\theta_j)}\right.$$

$$\left.+\sum_{j=M+1}^{2M} C_j \frac{1-\frac{r_{j-M}}{s}\cos(\theta_{i-M}-\theta_{j-M})}{1+\left(\frac{r_{j-M}}{s}\right)^2-\frac{2r_{j-M}}{s}\cos(\theta_{i-M}-\theta_{j-M})}-g^{\epsilon}(\cos(\theta_{i-M}),\sin(\theta_{i-M}))\right]^2$$

$$+\sum_{i=2M+1}^{3M}\left[\frac{1}{2}\sum_{j=1}^{M} C_j \ln[r_{i-2M}^2+R_{ext}^2-2r_{i-2M}R_{ext}\cos(\theta_{i-2M}-\theta_j)]\right.$$

$$\left.+\frac{1}{2}\sum_{j=M+1}^{2M} C_j \ln[r_{i-2M}^2+\left(\frac{r_{j-M}}{s}\right)^2-\frac{2r_{i-2M}r_{j-M}}{s}\cos(\theta_{i-2M}-\theta_{j-M})]\right]^2, \qquad (20)$$

and then differentiate this expression with respect to C_k for $k=\overline{1,2M}$ and r_l for $l=\overline{1,M}$ to explicitly find the gradient $\nabla S(\underline{C},\underline{r})$.

4 Numerical Results and Discussion

As a first example, example 1, we consider a simple two-dimensional detection of an unknown circular cavity $D=B_2(0, r_0)$ of radius $r_0 \in (0,1)$ within the unit circle $\Omega=B_2(0,1)$. We take $f = -\ln(r_0)$ on $\partial\Omega$ in (4) and then the direct problem given by equations (2)-(4), when $D=B_2(0,r_0)$ is known, has the unique solution

$$u(r,\theta)=\ln(r/r_0), \quad r_0 \leqslant r \leqslant 1, \qquad 0<\theta\leqslant 2\pi. \qquad (21)$$

The initial guess is taken as a circle located at the origin with radius 0.5 unless explicitly stated otherwise. This is typical for problems of this structure where a cavity is being located in a unit circle. Numerical results are presented for $R_{ext}= s =2$ and $M=N_I=30$. We have found that further refinements did not significantly improve the accuracy of the numerical results.

4.1 No noise

The cavity to be identified was located at the origin of radius $r_0=0.7$ and consider first the case when there is no noise added to the measured data (5), i.e. $\varepsilon=0$. Figure 1(a) shows the results obtained from the

minimisation routine following a series of 200 iterations. It can be clearly seen that the routine locates the cavity with a high accuracy as the result exactly overlays the analytical desired cavity. Figure 1(b) shows the objective function (20) as a function of the number of iterations. From this figure it can be seen that for the first 100 iterations the solution remains almost at the initial guess after which it drops for the next 100 iterations and finally it drops to zero after about a total of 200 iterations. Similar good results were obtained when we searched for cavities of radii 0.8, 0.6, 0.4, 0.3 or 0.2. Small errors in the final location accuracy arise when cavities of size 0.1 and below are attempted to be retrieved.

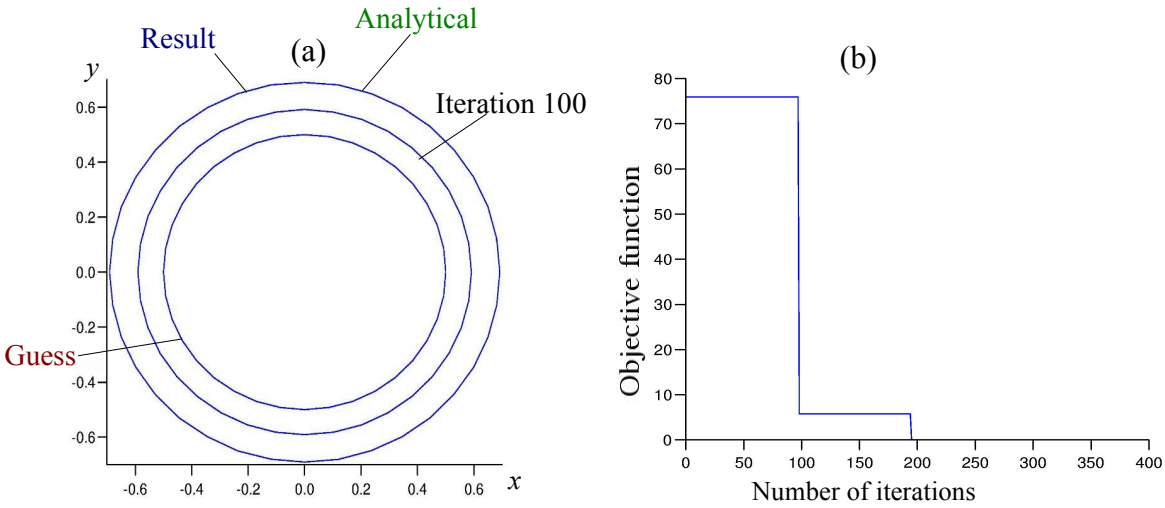

Figure 1: (a) The output from the minimisation routine for example 1 when searching for a circular cavity located at the origin of radius r_0=0.7, and (b) the objective function as a function of the number of iterations.

4.2 Adding noise to the boundary data

To simulate real measured data, random noise is introduced into the Neumann boundary data g as g^{ε} given by

$$g^{\varepsilon}(\underline{x}_i) = 1 + \varepsilon_i \,, \qquad i = \overline{1, M} \,, \tag{22}$$

where ε_i are Gaussian random variables with mean zero and standard deviation $\sigma = \rho\%$ = percentage of noise, generated using the NAG routine G05DDF. As expected, since the inverse cavity problem is ill-posed and no regularisation was included in the objective least-squares functional (13), the addition of noise to the data (22) gave inaccuracies and instabilities into the numerically obtained results even when very small amounts of noise were used.

4.3 Summary of the results obtained

The results obtained for example 1 show that the technique employed is capable of detecting circular cavities of various radii positioned at the origin of a unit circle when an initial guess of a circle of radius 0.5 located at the origin is used. Using this procedure enables circles as small as radii 0.2 to be located accurately when no noise is introduced in the input data. When noise is added into the normal derivative term (22), the routine fails to locate the cavity regardless of the mesh size employed. It is anticipated that the inclusion of a regularisation term into the objective function (13) will improve the stability of the results.

4.4 Incorporating a regularising term

Regularisation is necessary in order to obtain a stable solution when noisy data g^{ε} is used in (13). In this case we modify the functional S given by equation (13) by adding to it the regularisation term

$$T(\lambda_1, \lambda_2, \lambda_3, \underline{C}, \underline{r}) = \lambda_1 \sum_{j=1}^{2M} C_j^2 + \lambda_2 \sum_{j=1}^{M} r_j^2 + \lambda_3 \sum_{j=2}^{M} (r_j - r_{j-1})^2, \tag{23}$$

where $\lambda_1, \lambda_2, \lambda_3 \geqslant 0$ are regularisation parameters. The second term imposes the continuity of the boundary ∂D, whilst the third term imposes the smoothness $C^1$of the boundary ∂D. If the boundary ∂D is *a priori* known to be of class C^2 then (23) could include an extra term $\lambda_4 \sum_{j=3}^{M} (r_j - 2r_{j-1} + r_{j-2})^2$.

Also we can take $\lambda_2 = 0$ whenever $\lambda_3 > 0$ since the first-order regularisation includes the zeroth-order regularisation.

4.5 Results with regularisation

In the first instance we investigate results when $\lambda_3 = 0$ and $\lambda_1 = \lambda_2$, for the simplicity of having only one regularisation parameter to specify. Then, the regularisation term (23) becomes

$$T(\lambda_1, \underline{C}, \underline{r}) = \lambda_1 \left\{ \sum_{j=1}^{2M} C_j^2 + \sum_{j=1}^{M} r_j^2 \right\}. \tag{24}$$

The circular cavity to be identified was located at the origin of radius r_0=0.4. Figure 2(a) shows how the routine successfully locates the cavity as the result exactly overlays the analytical solution when no noise is used. Figure 2(b) shows the objective function when no noise is used and it can be observed that the function reaches approximately zero after 200 iterations.

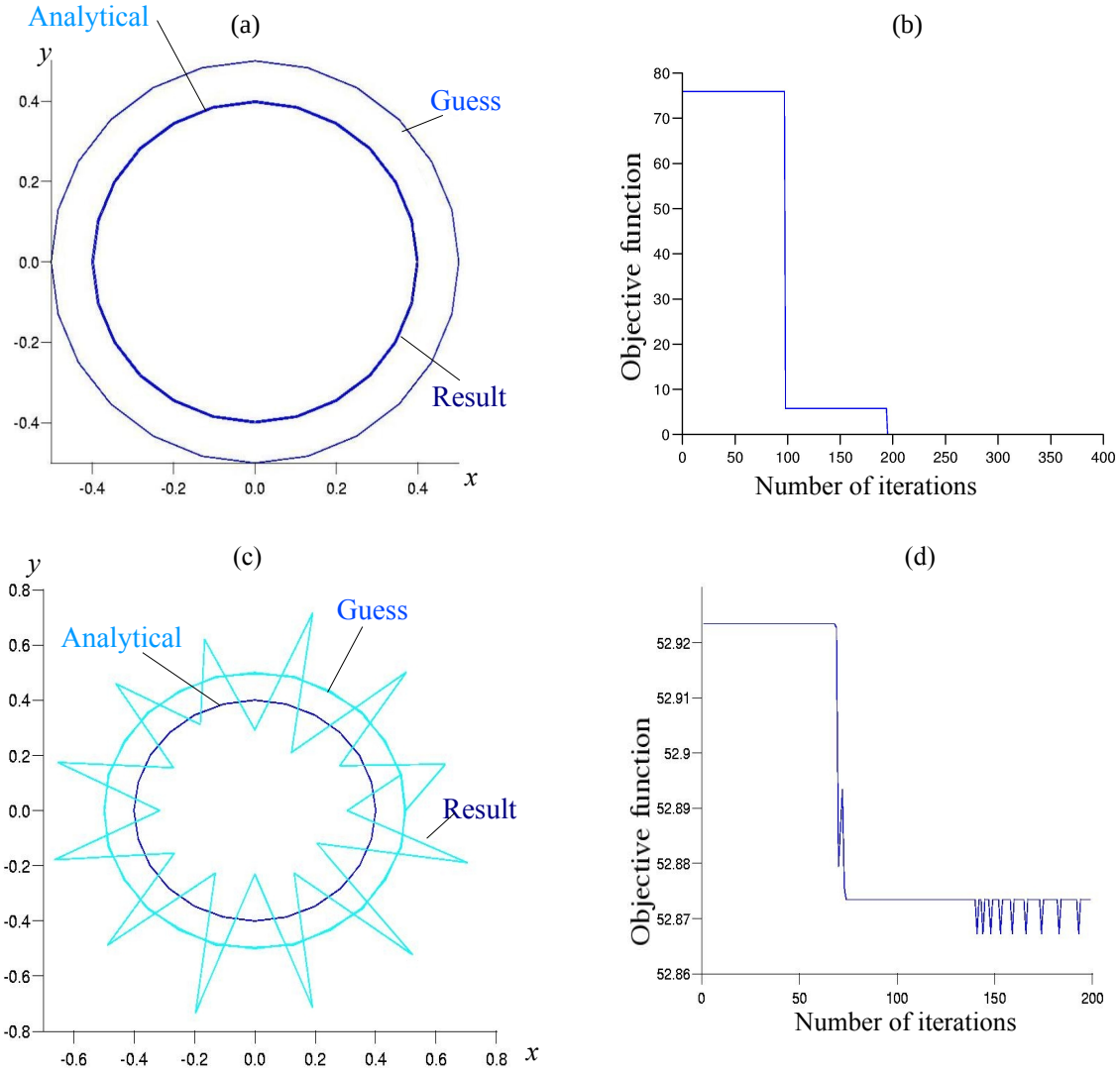

Figure 2: The output from the minimisation routine after the final iteration for example 1 when searching for a circular cavity located at the origin of radius r_0= 0.4 with the addition of (a) no noise, (b) the respective objective function, (c)1% noise, and (d) the respective objective function.

A meaningless result is obtained from the results of the minimisation routine when 1% noise is included in the data (22) and no regularisation is used, i.e. $\lambda_1 = 0$ in (24), see Figure 2(c). It can be observed in Figure 2(d) that, consistent with the cavity not being located, the objective function fails to minimise. The results for 5% noise were observed to have very similar characteristics to those of 1% noise. Figure 2(c) further illustrates the ill-posedness of the inverse problem and that classical direct methods are inappropriate to solve it.

Figure 3 shows the objective function obtained when the regularisation parameter $\lambda_1 = 0.05$ is used in

(24) for 1%, 3% and 5% noise. In comparison to Figure 2(d), it can be observed that the results are significantly improved with the objective functions approaching zero in each case. The smaller is the amount of noise, the faster the objective function approaches zero.

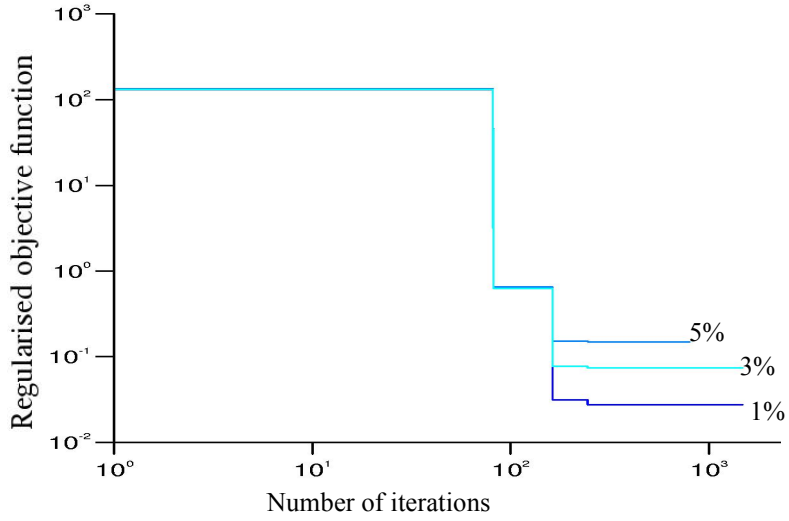

Figure 3: The regularised objective function for example 1, as a function of the number of iterations, with λ_1=0.05 for various amounts of noise 1%, 3% and 5%, when searching for a cavity located at the origin of radius r_0=0.4.

These objective function results are reflected in the accuracy of the cavity location. In Figure 4(a) it can be clearly observed that the cavity is located very accurately when 1% noise is employed and in Figure 4(b) the r_0=0.4 radius cavity is located with reasonable accuracy when 5% noise is used.

4.6 Searching for a range of cavity sizes

We have observed that the MFS successfully solves problems with noisy data by including a regularisation parameter for the case of locating cavities of radius 0.4, located at the origin. It is advantageous to validate the technique by attempting to locate other sizes of cavity.

A range of size cavities located at the origin with radii 0.2, 0.6, 0.8 were investigated. In the first instance, the value of the regularisation parameter is kept the same as in the previous example as this helps to indicate if the parameter is robust for a range of cavity sizes. Figure 4 (a) shows the results obtained when a regularisation parameter of $\lambda_1 = 0.05$ is used for 1% noise and Figure 4 (b) shows the equivalent result for 5% noise. It can be observed that the results demonstrate very high accuracy for the 1% noise. For 5% noise the large cavities are located with high accuracy, however this accuracy can be observed to reduce marginally as the cavity being located is reduced in size.

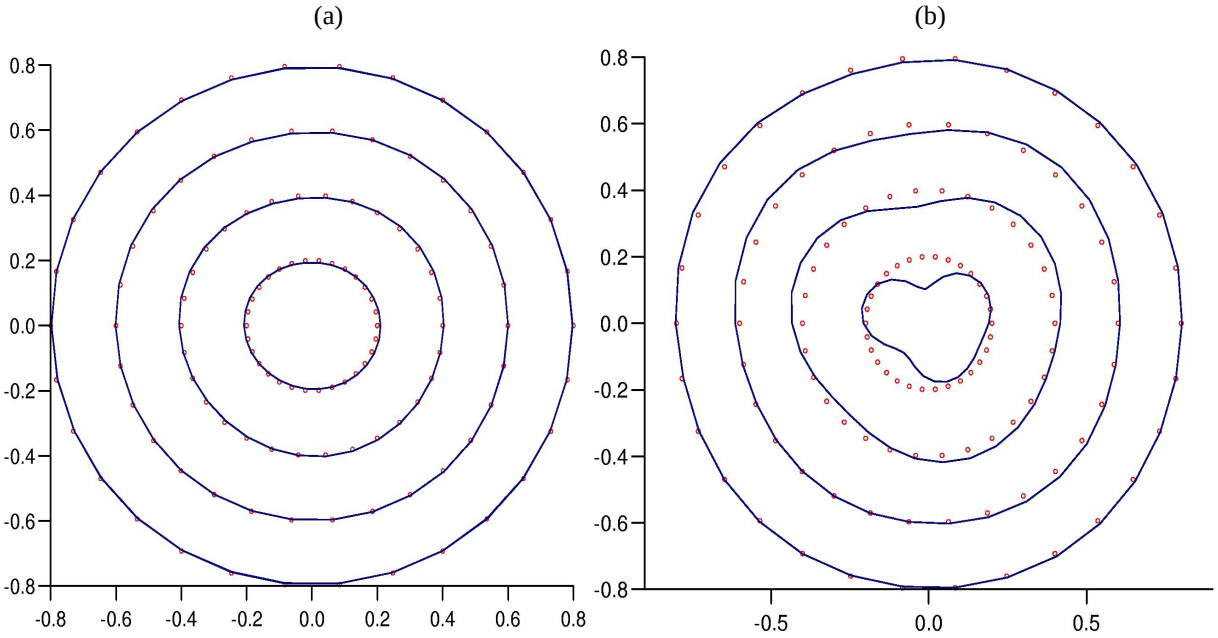

Figure 4: The output of the regularised minimisation routine for example 1 with λ_1=0.05 after the final iteration when searching for circular cavities of radii $r_0 \in \{0.2, 0.4, 0.6, 0.8\}$ *for (a) 1% noise, and (b) 5% noise. The dots represent the analytical targets whilst the continuous lines represent the numerical values retrieved.*

The robustness of the technique with the constant regularisation parameter are very encouraging for the MFS approach as they show that when using the same value of the regularisation parameter then multiple sizes of cavities can be located with a high level of accuracy, even when up to 5% noise is employed. Further values of λ_1 were investigated without any significant improvement in the results obtained for the 5% example. The successful implementation of the MFS technique for solving the inverse problem for a circular geometry provides confidence in validating for examples with more complex geometries.

4.7 Validating the approach for more complicated geometries

In this subsection we aim to locate cavities with more complicated geometries such as the bean shaped geometry in example 2, given by the parametrisation

$$(x(\theta), y(\theta)) = \frac{0.5 + 0.4\cos\theta + 0.1\sin 2\theta}{1 + 0.7\cos\theta}(\cos\theta, \sin\theta), \qquad \theta \in (0, 2\pi]. \tag{25}$$

Once again the initial guess is a circular cavity of radius 0.5 located at the origin. Unlike the previous case, see example 1, a non-analytical example is taken to specify the boundary conditions (3) and (4) as $u = 0$ on ∂D and $u = x$ on $\partial\Omega$. Since the required Neumann boundary data $\partial_n u|_{\partial\Omega}$ is not found analytically, the forward MFS procedure was implemented to calculate these values, as described in [Borman et al. 2007]. When using the data $g=\partial_n u|_{\partial\Omega}$ from the direct solver, noise was added to this data and a different M in the inverse procedure was used in order to avoid committing the inverse crime [Colton and Kress 1998]. A wide range of regularisation parameters were investigated. When either $\lambda_1=0$ or $\lambda_2=0$, a stable result could not be achieved. An observational approach based on trial and error found that the most reliable result was achieved when $\lambda_1=0.07$ and $\lambda_2=0.05$. Figure 5 shows the results obtained in this case when 0, 1% and 5% noise are used. It can be observed that the results are encouraging as for all noise levels a reasonable approximation to the bean shape is located. Further, the results are as accurate as numerical results obtained by [Ivanyshyn and Kress 2006] using a boundary integral approach.

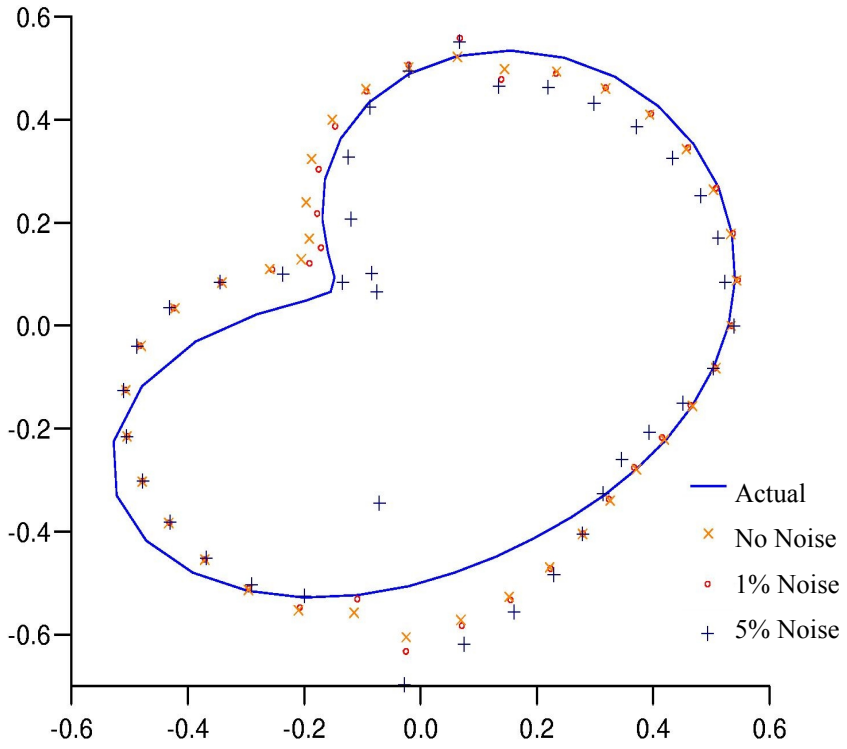

Figure 5: The output of the regularised minimisation routine for example 2 with $\lambda_1=0.07$ and $\lambda_2=0.05$ after the final iteration when searching for a bean shaped cavity given by equation (25). The continuous line represents the analytical target whilst the points represent the numerical values retrieved for no noise, 0, 1% and 5% noise.

5 Conclusions

It has been successfully demonstrated that the MFS procedure can be used to solve inverse problems, as a useful technique for locating obstacles from boundary data, as is the requirement in EIT. The numerical experiments exhibited very accurate results for exact data, but inaccurate results when noise was introduced if no regularisation was employed. The addition of a regularisation parameter was very successful and enabled cavities to be found in a stable way for 1-5% noise added into the Neumann boundary data. As might be expected intuitively, the larger cavities were located to higher accuracies in examples containing noise. Multiple star-shaped cavities can also be located in principle by applying the MFS to each cavity as described in Section 3.

Using the spherical parameterisation (9), a similar, but more tedious, analysis can be performed in three dimensions and this will be investigated as part of future work.

Acknowledgements

Duncan Borman would like to acknowledge the financial support for this work from the Rothschild scheme and the University of Leeds.

References

Alessandrini, G. and Rondi, L. (2001) *Optimal stability estimates for the inverse problem of multiple cavities*, J. Diff. Equations 176: 356-386.

Balakrishnan, K. and Ramachandran, P.A. (2000) *The method of fundamental solutions for linear diffusion-reaction equations*, Math. Comput. Modelling 31: 221-237.

Bogomolny, A. (1985) *Fundamental solutions method for elliptic boundary value problems*, SIAM J. Numer. Anal. 22: 644-669.

Barber, D. and Brown, B. (1984) *Applied tomography,* J. of Phys. E:Sci. Instrum. 17: 723 -733.

Boone, K. (2006) *Introduction to Electrical Impedance Tomography*, www.EIT.org.uk, Department of Clinical Neurophysiology, Middlesex Hospital.

Borcea, L. (2002) *Electrical impedance tomography*, Inverse Problems 18: R99-R136.

Borman, D., Ingham D. B., Johansson, T. and Lesnic, D. (2007), *The method of fundamental solutions for direct cavity problems in EIT*, in Advances in Boundary Integral Methods - Proceedings of the Sixth UK Conference on Boundary Integral Methods, (ed. J. Trevelyan), Ch. 21, 193-202.

Burgess, G. and Mahajerin, E. (1984), A comparison of the boundary element method and superposition methods, Comput. Struct. 19:697-705.

Colton, D. and Kress, R. (1998) *Inverse Acoustic and Electromagnetic Scattering Theory*, 2nd edn., Springer-Verlag, Berlin.

Duraiswami, R., Chahine, G. L. and Sarkar, K. (1997) *Boundary element techniques for efficient 2-D*

and 3-D electrical impedance tomography, Chem. Eng. Sci. 13: 2185-2196.

Fairweather, G. and Karageorghis, A. (1998) *The method of fundamental solution for elliptic boundary value problems,* Adv. Comput. Math. 9:69-95.

Goldberg, M. A. and Chen, C. S. (1999) *The method of fundamental solutions for potential, Helmholtz and diffusion problems*, in Boundary Integral Methods: Numerical and Mathematical Aspects, Comput. Mech. Publ., Southampton, 103-176.

Haddar, H. and Kress, R. (2005) *Conformal mappings and inverse boundary value problems*, Inverse Problems 21: 935-953.

Hanke, M. and Bruhl, M. (2003) *Recent progress in electrical impedance tomography,* Inverse Problems 19: S65-S90.

Holder, D. (2005) *Electrical Impedance Tomography: Methods, History and Applications*, Institute of Physics, Bristol.

Ivanyshyn, O. and Kress, R. (2006) *Nonlinear integral equations for solving inverse boundary value problems for inclusions and cracks*, J. Integral Equations Appl. 18:13-38.

Johnston, R. L. and Fairweather, G. (1982) *The method of fundamental solutions for problems in potential flow,* Appl. Math. Modelling 8: 265-270.

Kim, S., Kwon, O. and Seo, J. K. (2002) *Location search techniques for a grounded conductor,* SIAM J. Appl. Math. 62:, 1283-1293.

Kress, R. (2004) *Inverse Dirichlet problem and conformal mapping,* Math. Comput. Simulation 66: 255-265.

Smith, J. R. (1996) *Field mice: extracting hand geometry from electrical field measurements*, IBM Systems J. 35:587-608.

Smith, J.R., White, T., Dodge, C., Paradiso, J., Gershenfeld, N. and Allpost, D. (1998) *Electric field sensing for graphical interfaces*, IEEE Computer Graphics Appl. 18: 54-60.